Spatially Distributed Hydrological Modelling

Wetness Derived from Digital Elevation Models to Estimate Peatland Carbon

Hasan, Abdulghani

2012

Document Version:
Publisher's PDF, also known as Version of record

Spatially Distributed Hydrological Modelling

Wetness Derived from Digital Elevation Models to Estimate Peatland Carbon

Hasan, Abdulghani

2012

Spatially Distributed Hydrological Modelling

Wetness derived from digital elevation models to estimate peatland carbon

LUND
UNIVERSITY

Abdulghani Hasan

Centre for Geographical Information Systems (GIS Centre)
Department of Physical Geography and Ecosystem Science
Lund University, Sweden 2012

A doctoral thesis at a university in Sweden is produced either as a monograph or as a collection of papers. In the latter case, the introductory part constitutes the formal thesis, which summarizes the accompanying papers. These have either already been published or are manuscripts at various stages (in press, submitted or in manuscript)

ISBN 978-91-85793-28-0

Printed in Sweden by Media-Tryck, Lund University
Lund 2012

List of papers

I Hasan, A., Pilesjö, P., & Persson, A. (2012) On generating digital elevation models from LiDAR data – resolution versus accuracy and topographic wetness index in northern peatlands, Geodesy and Cartography, Taylor & Francis. (Accepted)

II Pilesjö, P., & Hasan, A. A triangular form-based multiple flow algorithm to estimate overland flow distribution and accumulation on a digital elevation model. (Submitted)

III Hasan, A., Pilesjö, P., & Persson, A. (2012) Drainage Area Estimation in Practice - how to tackle artefacts in real world data, GIS Ostrava 2012 - Surface Models for Geosciences, 23-25 January 2012, Ostrava, Czech Repubic.

IV Persson, A., Hasan, A., Tang, J., & Pilesjö, P. (2012) Modelling Flow Routing Patterns in Permafrost Landscapes with Topographical Wetness Index, Transactions in GIS, Wiley. (Accepted)

V Hasan, A., & Persson, A. Distributed Modeling of Active Layer Thickness with Soil Moisture from a Topographic Wetness Index. (Manuscript)

Contribution to the papers

I Study design, programming, data analysis, and contribution to manuscript writing.

II Study design, programming, data analysis, and contribution to manuscript writing.

III Contribution to study design, fieldwork, programming, data analysis, and contribution to manuscript writing.

IV Contribution to study design, fieldwork, programming, and data preparation.

V Study design, programming, fieldwork, data analysis, and manuscript writing.

Abstract

To study the hydrology of peatlands and explore wetness distribution is difficult mainly due to the complexity of the surface of peatlands, and also due to the presence of permafrost underlain peatlands in the arctic regions. I have chosen the area called Stordalen mire in the arctic region in northern Sweden for my study.

In this thesis, I aimed to study spatially distributed hydrological modelling in general, focusing mainly on evaluation and developing tools that can be used to improve wetness estimation using Digital Elevation Models (DEMs). The estimated wetness can be used as an input for peatland carbon models.

DEMs with different resolutions are created using high resolution LiDAR data. Different search radiuses are used in the interpolations. The accuracy of the generated DEMs is studied to select the most accurate DEM for each selected resolution. The search radius, but not the cell size, significantly influences the accuracy of a DEM, and the accuracy is generally higher the shorter the interpolation search radius. DEM resolution versus topographic wetness index variables (i.e. slope and drainage area) is studied. Slope values become lower and drainage area values become higher when the resolution decreases. Further, a study of DEM accuracy related to different slopes is also carried out and shows that the errors in elevation are greater when the terrain is steep than when it is flat.

A new triangular form-based multiple flow distribution and flow accumulation algorithm (TFM) was created in this study. We have estimated flow distribution by using our new TFM algorithm. With this TFM algorithm, it becomes possible to deal with artefacts that normally interrupt flow distribution, like flat areas, sinks and man-made structures. This will help to overcome the complexity of peatland hydrology. The results of comparing our new algorithm with other well-known algorithms used in most GIS programs show that the TFM algorithm produces more realistic results than other algorithms. Testing shows the capability of the new TFM algorithm to distribute the flow in different terrain types, flat areas and sinks, and makes it suitable for simulating real flow distribution over any surface/terrain.

Topographic wetness index (TWI) was estimated for the study area using our new flow distribution and flow accumulation algorithm TFM. Estimating TWI values depending only on DEMs is a very cost-effective method that can be used to estimate wetness data required for the modelling of peatlands. A permafrost model was created to demonstrate the possibility of using an analytically based approach with semi-empirical equations to estimate the maximum thawing depth (active layer thickness) above permafrost. Field work using water level sensors was carried out to measure the

temporal fluctuation of water surface. The field work water level measurements led to better understanding of flow regime in the peatlands, especially when a seasonally frozen layer or permafrost lies under it. The field work also helped to confirm that estimated wetness using the proposed flow routing algorithm on digital elevation model can be used to distribute wetness to all cells in a DEM.

Keywords: modelling hydrology, digital elevation models, topographic wetness index, LiDAR data, peatland, permafrost, Stordalen.

Svensk sammanfattning

Hydrologiska studier i torvmarker, inkluderat undersökningar avseende rumslig fördelning av markfuktighet, är ofta svåra att genomföra. Huvudanledningen till detta är torvmarkernas komplexa hydrologi beroende på dess heterogena yta, men även påverkan av permafrost, vilken är väl utbredd i arktiska regioner. I detta arbete har Stordalens myr i norra Sverige studerats med avseende på hydrologi.

Syftet med avhandlingsarbetet har varit att studera rumsligt distribuerad hydrologisk modellering med hjälp av digitala höjdmodeller. Fokus har legat på att utvärdera befintliga modeller, samt på att utveckla nya verktyg för att kunna förbättra skattningar av markfuktighet. Huvudsyftet med att skatta markfuktigheten är att den skall kunna användas i kolmodeller anpassade till torvmarker.

Digitala höjdmodeller med olika rumslig upplösning har på olika sätt skapats utifrån högupplösande LiDAR-data. Noggrannheten i de skapade modellerna har undersökts för att kunna välja optimal höjdmodell för varje upplösning. Man kan konstatera att sökradien vid interpolationen, men inte den rumsliga upplösningen (cellstorleken), påverkar noggrannheten i modellen, samt att noggrannheten generellt är bättre ju kortare sökradie som används. Även förhållandet mellan höjdmodellers rumsliga upplösning och olika faktorer som påverkar markfuktighet, nämligen sluttningslutning och dräneringsarea, har studerats. Slutsatsen är att den skattade sluttningslutningen minskar, och den skattade dräneringsarean ökar, när den rumsliga upplösningen minskar. Även en studie avseende eventuella samband mellan höjdmodellers noggrannhet och skattad sluttningslutning har genomförts. Resultaten visar att höjdfelen är större i kuperad terräng med branta sluttningar än på planare mark.

En ny formbaserad algoritm för skattning av ytvattenflöde och flödesackumulation över digitala höjdmodeller, baserad på triangelnät och multipla flödesriktningar, har uvecklats inom detta arbete. Ytvattenflöden över såväl naturliga som matematiskt genererade höjdmodeller har skattats med hjälp av den nya algoritmen. Även funktioner för att vid skattningen kunna behandla artefakter som platta ytor, små isolerade dräneringsområden, samt spår av mänsklig aktivitet (t.ex. kulvertar), har inkluderats i algoritmen. Detta ökar möjligheterna att modellera ytvatten i topografiskt komplexa torvmarker. Jämförelser mellan den nyutvecklade algoritmen och andra välkända och frekvent använda algoritmer visar klart att den förstnämnda producerar mer realistiska resultat. Tester visar den nyutvecklade algoritmens kapacitet att skatta ytvattenflöden i olika typer av terräng, samt över platta ytor och i

små isolerade dräneringsområden. Detta gör den lämplig för användning inte bara i torvmarker, utan i alla områden.

Ett topografiskt fuktighetsindex, baserat på den nyutvecklade algoritmen, har skattats över hela undersökningsområdet. Att skatta fuktighet uteslutande på grundval av digitala höjdmodeller är en förhållandevis kostnadseffektiv metod, och kan bli betydelsefull för modellering av hydrologiska förhållanden i bland annat torvmarker. Även en modell för skattning av djup till permafrost, så kallat aktivt lager, har skapats inom detta arbete. Syftet med detta var att demonstrera möjligheten att använda en analytisk metod med (semi-)empiriska ekvationer för att skatta rumslig fördelning av permafrost. Fältmätningar av grundvattenyta och det aktiva lagret har genomförts, vilket gett ökad förståelse av hydrologin i torvmarker. Fältarbetet har även bekräftat att den ovan nämnda utvecklade algoritmen för skattning av markfuktighet ger ett realistiskt resultat. Den kan med fördel användas för att skatta den rumsliga fördelningen av markfuktighet utifrån en digital höjdmodell.

Acknowledgments

I would like to express my gratitude and the deepest appreciation to my supervisor Petter Pilesjö, who has the attitude and the substance of a genius: he continually and convincingly conveyed a spirit of adventure in regard to research. I have been extremely lucky to have a supervisor who cared so much about my work, and who responded to my questions and queries so promptly. Without his guidance and persistent help this dissertation would not have been possible. I am also thankful to my second supervisor Andreas Persson who was abundantly helpful and offered invaluable assistance, support and guidance.

I cannot find words to express my gratitude to all my colleges at the GIS Centre, (Karin, Ulrik, Micael, Lars, Roger, Mitch, Hanna, Helena, Mojgan, Jing, Irene, Ali and Ara), I consider it an honour to work with you.

I would like to thank all my colleges, graduate students, professors, teachers, and administration staff at the department of physical geography and ecosystem sciences, my special thanks goes to Patrik Vestin, Per Schubert, Jonathan Seaquist, Sadegh Jamali, and Petra Andersson.

It gives me great pleasure in acknowledging the support and help of Professor Nigel Roulet, Department of Geography, McGill University.

Thanks for a never ending support from my parents, my sisters, and my brothers. I must express my gratitude to my wife, for her continued support and encouragement also to my lovely daughters and son (Aleen, Waseem, Reem, and Basma).

This study is funded by the European Union funding programme Erasmus Mundus "External Cooperation Window" (EMECW lot8), and also by Lund university.

Abbreviations

Abbreviation	Description
DEM	Digital Elevation Model
SFD	Single Flow Direction
MFD	Multiple Flow Direction
TWI	Topographic Wetness Index
ALT	Active Layer Thickness
WTD	Water Table Depth
TFM	Triangular Form-based Multiple flow distribution algorithm
SSW	Site Specific Wetness
D8	Single direction flow distribution algorithm
MD8	Multiple Direction flow distribution algorithm
D∞	Triangular single direction flow distribution algorithm
MD∞	Triangular multiple direction flow distribution algorithm
DEMON	Digital Elevation Model Networks flow distribution algorithm
DOC	Dissolved Organic Carbon
NMAD	Normal Median Absolute Deviation
LiDAR	Light Detection And Ranging

Table of Contents

1. Introduction

1.1. Peatlands, permafrost and global climate change

The mean annual air temperatures in regions north of 65° N have increased by about 2–3 ºC since the 1950s, which is almost twice the rate of the rest of the world (ACIA, 2005). The predicted temperature raise may equal to two to three times greater than the global average as it is indicated by climate change scenarios for the arctic regions. One of the most important environmental and socioeconomic impacts of temperature rise is the melting of permafrost (Zhang et al., 2003).

Permafrost distribution in the subarctic region is discontinuous and patchy, and occurs mainly as palsas (peat mounds with a permanently frozen core), but also as elevated permafrost plateaus, formed in subarctic mires (Woo, 2012). The peat serves as a large storage of carbon that has been accumulated over thousands of years. Once the soil starts to thaw, carbon previously stored as frozen peat is released and 'lost' through microbial activities (CO2 and CH4), as well as through transportation of dissolved organic carbon (DOC), by percolated water to surrounding streams (Olefeldt and Roulet, 2012). The rates at which these carbon losses occur depend on microbial activity (soil temperature), soil wetness, vegetation cover, and active layer thickness.

Subarctic permafrost demarcates the outer border of permafrost existence, and is highly sensitive to altered climate conditions (Bosiö et al., 2012). Even modest changes in micro-topography and vegetation patterns due to thawing permafrost will affect drainage and snow accumulation, which in turn may enhance permafrost degradation. Hence, when modelling climate-hydrological interactions in these environments it is necessary to take into account the scale of individual peat mounds and hollows, which requires high spatial resolution. It is essential to measure and model the thickness of the seasonally thawed layer above the permafrost as this will lead to estimating all feedbacks which accompany the thawing process.

1.2. Hydrologic processes of peatlands

Hydrology of Peatlands underlined by permafrost is the study of distribution, movement, and storage of water as this is directly or indirectly affected by the presence of perennially frozen ground (Woo, 2012). Many different hydrological processes may occur where permafrost exists; one example of those processes is how water is transported in continuous permafrost areas. The rapid runoff and the overland flow are very common phenomena because of the relatively impervious permafrost layer (Hinzman et al., 2006). For the discontinued permafrost zone (more related to this study), the hydrologic processes are even more complicated and will be further investigated and discussed in this study.

The cycling of carbon and the ecological function of northern peatlands are direct consequences of their hydrological condition. Persistently wet conditions result in accumulation of dead plant material in the form of peat, and the production and emission of CH_4. These conditions make peatlands relatively unique as a source or sink for two greenhouse gases, CO_2 and CH_4 (Frolking and Roulet, 2007).

The peatland hydrology is crucial for climate change impacts, and the estimations of emissions from coupled models are still crude, lacking tested modules, e.g. the hydrological-permafrost-methane link for northern peatlands. To include such a feedback loop into the models requires a new processed based rule set that works on a relevant scale. Today these processes are parameterized on a scale that is far from the high resolutions needed to capture the results (Wania et al., 2010; Baird et al., 2009).

Since the water content value is different from point to point and is highly dependent on the slope and topography (Famiglietti et al., 1998), modelling water accurately is very important for accurate, active layer thickness estimations. A dynamic, distributed model is presented in this study to model the effect of thawing permafrost on local topography, and active layer thickness. The permafrost model in this study was applied to a subarctic mire named Stordalen mire near Abisko scientific research station north of Sweden.

As mentioned in section 1.1, most climate scenarios suggest that higher latitudes will experience greater temperature increases and more winter precipitation than the global mean increase. This will likely lead to an increase of the permafrost active layer, which in turn is likely to have a profound effect on surface hydrology.

When permafrost melts, the surface of the peatlands tends to drop relatively to the surrounding landscape, significantly increasing the local wetness of the peatland. This often results in a structural change of the peatland ecosystem from a relatively dry

raised peatland plateau to a much wetter mineral poor fen. Figure 1 clarifies the process of increasing local wetness due to the thawing process.

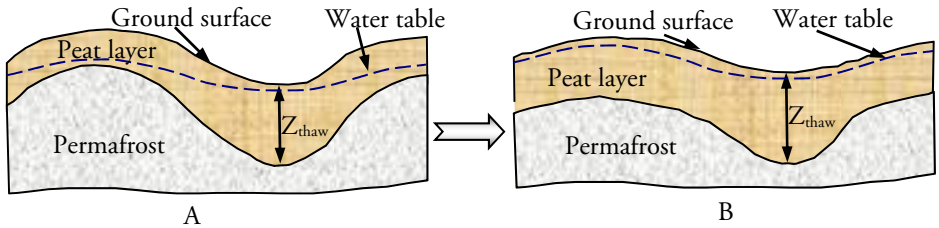

Figure 1. Soil cross section with peat and permafrost layers; A) Current state. B) Increasing local wetness due to thawing of permafrost and increasing the active layer thickness.

1.3. Surface flow algorithms over digital elevation models (DEM)

A digital elevation model DEM is a regularly spaced grid with height information in each grid cell. The DEM is a 3D model of the terrain, which means that it is an approximation of a real surface and may contain errors. The accuracy of any created DEM (to represent the real surface) depends on many factors, e.g. data collection method, data density, interpolation algorithm, grid resolution, and slope variability (Höhle and Höhle, 2009).

During the last three decades, a large number of various flow routing algorithms has been developed to simulate flow distribution over digital elevation models (DEMs) (Zhou et al., 2008). Each surface flow distribution and accumulation algorithm may distribute the flow using different approaches and methodologies, and may differently deal with the artefacts that normally exist in any DEM (Zhou and Liu, 2002). In the following two sections a general presentation of surface flow distribution and accumulation algorithms, and the artefacts, are to be presented.

1.3.1. Single and multiple surface flow algorithms

Generally, surface flow distribution and accumulation algorithms can be based on either single flow direction (SFD) or multiple flow directions (MFD). If working with DEM raster data, the flow from any cell has eight different possible directions. The first SFD algorithm, known as Deterministic Eight-Node (D8), is presented by

(O'Callaghan and Mark, 1984). Another SFD algorithm is the Deterministic Eight-Node Least Transversal Deviation (D8-LTD), presented by Orlandini et al. (2003). With a SFD algorithm, 100% of the flow will be transported from any cell to just one adjacent cell, and is normally transported to the cell in the direction of the steepest downhill slope (Fairfield and Leymarie, 1991; O'Callaghan and Mark, 1984; Orlandini et al., 2003; Parsons and Abrahams, 1992). SFD algorithms are over-simplified and must be considered illogical, and would obviously create significant artefacts in the results as stated e.g. by Freeman (1991), Holmgren (1994), and Wolock and McCabe (1995).

With the multiple flow distribution algorithms, the flow from any cell can be transported to more than one cell, and up to a maximum of eight directions. The flow is normally distributed to all lower elevation cells in different directions with portions depending on the slope as explained in Equation 1. Examples of multiple flow distribution algorithms which distributing the flow according to Equation 1 are Freeman Multiple Flow Direction (FMFD) (Freeman, 1991), and Quinn Multiple Flow Direction (QMFD) (Quinn et al., 1991).

$$f_i = \frac{(\tan \beta_i)^x}{\sum_{j=1}^{8} (\tan \beta_j)^x} \qquad \text{, for all } \beta > 0 \qquad (1)$$

where i,j = flow directions (1…8), fi = flow proportion (0…1) in direction i, $\tan \beta_i$ = slope gradient between the centre cell and the cell in direction i, and x = variable exponent.

Using Equation 1 to weight the influence of slope when splitting flow between neighbouring cells is the main problem of MFD algorithms. By changing the exponent (x) in Equation 1, two extreme approaches in estimating flow distribution can be observed. While x = 1, flow will be distributed to downhill neighbouring cells proportionally to the slope gradients, as suggested by Quinn et al. (1991). The other extreme is when $x \rightarrow \infty$, which will approach towards the 'single flow' drainage distribution mentioned above. This exponent can thus be seen as a parameter that causes a gradual transition from SFD (infinite x; in practice values above 25) to slope proportional MFD (x=1). Holmgren (1994) suggested an x value between 4 and 6. This gives a result between a very homogeneous flow distribution when x = 1, and a distinctive flow which occurs when x becomes greater than 10. (Seibert and McGlynn, 2007) suggested using Triangular Multiple Flow Direction (MD∞) as a MFD algorithm to distribute the flow depending on triangular facets. Two examples of MFD that can be considered (partly) vector based algorithms are Digital Elevation

Model Networks (DEMON), (Costa-Cabral and Burges, 1994), and Triangular Facet Network (TFN), (Zhou et al., 2011).

1.3.2. Artefacts in the landscape

Large improvements in flow estimation have been made during the last decades. Most, if not all, of the proposed algorithms have been developed and tested on mathematical, or manipulated natural, surfaces. There is an urgent need to develop algorithms (or practical solutions) dealing with natural and artificial artefacts in the landscape, like flat areas and depressions (sinks). Such artefacts are caused by man, generalisation (of data type), or by errors in e.g. interpolation.

Sinks often need to be filled before estimating flow distribution. It should be noted that any unfilled sink will result in stopping flow at that sink/cell. Sometimes this is not desirable. It would be better if the filling sinks, additional to other knowledge, could be based on size and form of the sinks. Area, volume as well as depth of a sink might help the user to decide if it should be removed or not.

Tunnels and culverts are normally not captured within the data collection, and thus not included in the terrain model. A DEM covering an area including man-made barriers may thus result in non-natural sinks close to these structures. The barriers are often roads and railways, where structures like culverts, siphons and tunnels have been hidden when constructing the DEM. The resulting sinks should be removed since, in these cases, all cells are actually connected and the flow should continue through the culvert beneath the man-made artefact. It is thus crucial to identify cells on both sides of the artefact, and let water flow between these points e.g. by breaching the barrier. Such connecting flow structures cannot normally be detected in the data when creating DEMs.

Solving problems related to the quality of DEMs, and to use appropriate flow routing algorithms are crucial in hydrological modelling, and will lead to better representation of real world hydrological processes.

1.4. Topographic wetness index (TWI)

The topographic wetness index (TWI) concept was first introduced by (Beven and Kirkby, 1979) within the runoff model TOPMODEL. The effect of topography on runoff generation can be linked to TWI. TWI serves as a physically-based index approximating the location of zones of surface saturation and the spatial distribution

of soil water (Barling et al., 1994; Beven and Kirkby, 1979; O'Loughlin, 1986). TWI is widely used in many applications, like studies of spatial scale effects on hydrological processes (Beven and Jakeman, 1988; Famiglietti and Wood, 1991; Sivapalan and Wood, 1987), and in precision agriculture (Schmidt and Persson, 2003), as well as to identify hydrological flow paths for geochemical modelling (Robson et al., 1992), forest site quality (Holmgren, 1994), and vegetation patterns (Moore et al., 1993).

For the calculation of TWI a gridded DEM can be used. The calculation of TWI value is estimated using Equation 2.

$$TWI = \ln\left(A / \tan\beta\right) \quad (2)$$

where A is the upslope contributing specific catchment area (calculated by dividing total upslope area draining through a certain point by width of flow), and tan β is the slope gradient in the direction of flow.

TWI is influenced by the algorithm used to estimate the upslope contributing area (A), and the method used to estimate the slope gradient tan β (Guntner et al., 2004).

On a continental and regional scale Curmi et al. (1998), Gedney and Cox, (2003), and Kirkby et al. (1995) used TWI for modeling peatlands. They achieved better modelled results when they used higher resolution DEM. In small and medium-sized catchments, models have been proven to work well for resolutions high enough to capture the wetlands. Rodhe and Seibert (1999) showed that a too coarse resolution (>50m) will affect the result negatively in both wetland occurrence modelling and wetness estimations. The resolutions in their studies are, however, too coarse for the biogeochemical processes occurring in peatland complexes. The scales important to wetlands are defined by Baird et al. (2009) as the microtopography (1m scale), the mesotopography (10m scale) and the general morphology (100 to 1000m scale). The microtopography (1m scale) is necessary to detect the hollows and hummocks in peatlands. For the peatland as a whole, which to a large extent is a product of the hydrological conditions, the modelled TWI with the mesotopography (10m scale) may be used to separate different type of areas. This is not only valid for areas that are distinctly different like the fen (wet parts of peatlands), and the palsa (dry parts of Peatlands), but also for intermediate peatland conditions as the internal fen.

1.5. Objective and aims of the thesis

The main objective of this thesis is to study, evaluate and develop tools that can be used to improve wetness estimation for peatlands using Digital Elevation Models (DEMs).

In order to achieve this objective a number of specific aims are defined:

1. To evaluate the accuracy of the predicted elevation in different resolution DEMs, created from LiDAR data, using LiDAR data points as 'ground truth'.
2. To create a new flow distribution algorithm that can better simulate natural flow and overcome artefact problems.
3. To study how estimated slope and drainage area varies with DEM resolution and to conclude how estimated Topographic Wetness Index (TWI) then might vary with different DEM resolution.
4. To study how soil wetness represented by TWI can be used to reflect Site Specific Wetness (SSW), and also the thawing of Active Layer Thickness (ALT) above the permafrost in a Peatland.
5. To investigate the potential of modelling hydrological conditions on a permafrost underlain mire by the use of topographical wetness index.

2. Materials and methods

2.1. Study area

The study is based on earth surface elevation data and fixed observations measured at the Stordalen mire and its catchment area. Stordalen is a peatland area in the Arctic region 10 km west of Abisko scientific research station (68º 20' N, 19º 03' E) in northern Sweden. Figure 2 is a hill-shade of the used DEM covering the Stordalen area.

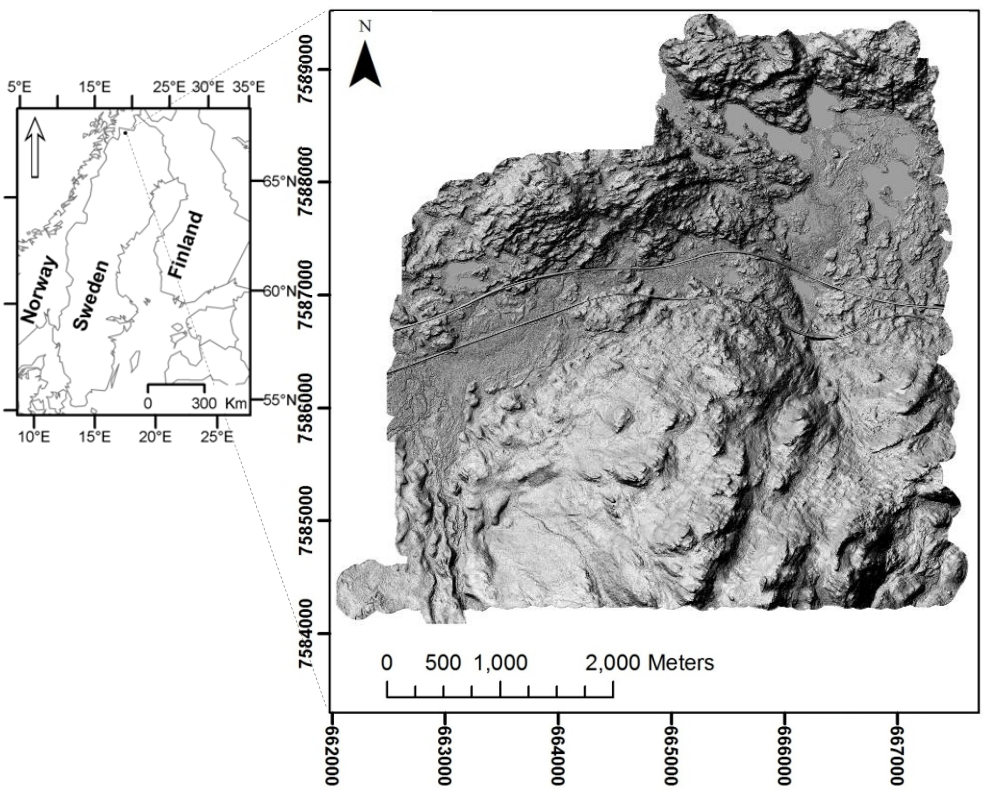

Figure 2. Hill-shade of the used DEM with location map of the study area (Stordalen mire and its catchment) close to Abisko scientific research station, in northern Sweden. (Hill-shade is in SEREFF99).

The hydrology and soil moisture conditions of the Stordalen mire have been described and documented previously by Rydén et al. (1980). The mean annual temperature for the period 1913-2003 was -0.7 °C for Abisko (Table 1), (Johansson et al., 2006). A regional rain shadow affects the precipitation and makes it among the lowest in Scandinavia, with a mean annual precipitation of 304 mm for the period 1913-2003 (Table 1), (Johansson et al., 2006). Apart from studies associated with the International Biological Program (IBP) (see e.g. Sonesson et al., 1980), the Stordalen area has been included in many research programs, and its climatological records extend from 1913 to the present date (Andersson et al., 1996). The peatland in the Stordalen area is a palsa complex, including fen areas, and permafrost underlain palsa bog areas. The thawing permafrost in the palsa bog part has led to the collapse of the palsa structure and a moister surface in this part (called the 'internal fen'). The permafrost active layer depth has been measured since 1978 (Christensen et al., 2004; Akerman and Johansson, 2008). Data on the waterborne export of carbon from the Stordalen catchment has also been correlated with TWI for the catchment as a whole (Olefeldt and Roulet, 2012). This site is thus suitable for investigating methods of estimating changes in carbon storage, providing the possibility of validating tools for the prediction of changes in peatlands with past and future changes in permafrost. An area of approximately 18 km^2, containing the Stordalen mire, was selected as the study area in this project.

Table 1. Climate characteristics measured at Abisko Scientific Research Station (ANS) for the study years 1970 and 2000, and the long term mean (1913–2003), (Johansson et al., 2006).

Year		TA	T′
1970	°C	-0.9	-0.2
2000	°C	0.5	1.2
1913-2003	°C	-0.7	
Year		PT	PT′
1970	mm	242.0	-61.3
2000	mm	359.0	55.7
1913-2003	mm	303.3	

TA, mean annual air temperature; T′, temperature anomaly from long time mean; PT, accumulated precipitation; PT′, precipitation anomaly from the long time mean.

2.2. Organization of the study

The study is organized to cover all the listed specific aims (see section 1.5). Each paper in this study is targeting one or more of those specific aims. As illustrated in Figure 3, the work within each paper is represented with different colour shading.

Paper I (colour light red in Figure 3). The study started with measuring surface elevation of our study area using an airborne LiDAR device. DEMs with different resolutions, and search radius are generated from the LiDAR data. Accuracy of the generated DEMs is studied to select the most accurate DEM for each selected resolution. DEM resolution versus topographic wetness index in northern peatlands, and the relation between slope and drainage area estimation and DEM resolution is studied. Further, a study of DEM accuracy related to different slopes is also conducted.

Paper II (colour light purple in Figure 3). A new triangular multiple flow distribution (TFM) algorithm is created. The new TFM algorithm is tested for flow distribution over DEMs using mathematical standard surfaces, and also using real world data. The new TFM is compared with other already existing SFD and MFD algorithms.

Paper III (colour light blue in Figure 3). Problems related to flow distribution algorithms are discussed. Solutions are presented to deal with natural and artificial artefacts in DEMs. A multiple flow distribution solution for estimating flow directions in flat cells is presented. A new interactive solution to fill sink cells depending on their volume, width, and depth is also performed. Artificial artefacts in the DEMs, like man-made structures are solved by breaching them with a culvert function. The problem of the exponent value (x) in Equation 1 is studied and discussed.

Paper IV (colour light orange in Figure 3). Water table fluctuation and active layer thickness (ALT) are measured in the field to study moisture pattern and site specific wetness (SSW) in peatlands. Field measurement values for SSW are compared with the TWI values estimated with our new TFM algorithm.

Paper V (colour light green in Figure 3). A distributed permafrost hydrologic model is created to estimate the ALT for all cells in a DEM. Multiple data layers are used as input to the permafrost hydrologic model. The results from papers I, II, III, and IV contributed in estimating TWI as one of the important input layers. Other external input data, not related to this study, are presented in Figure 3 with a light grey colour.

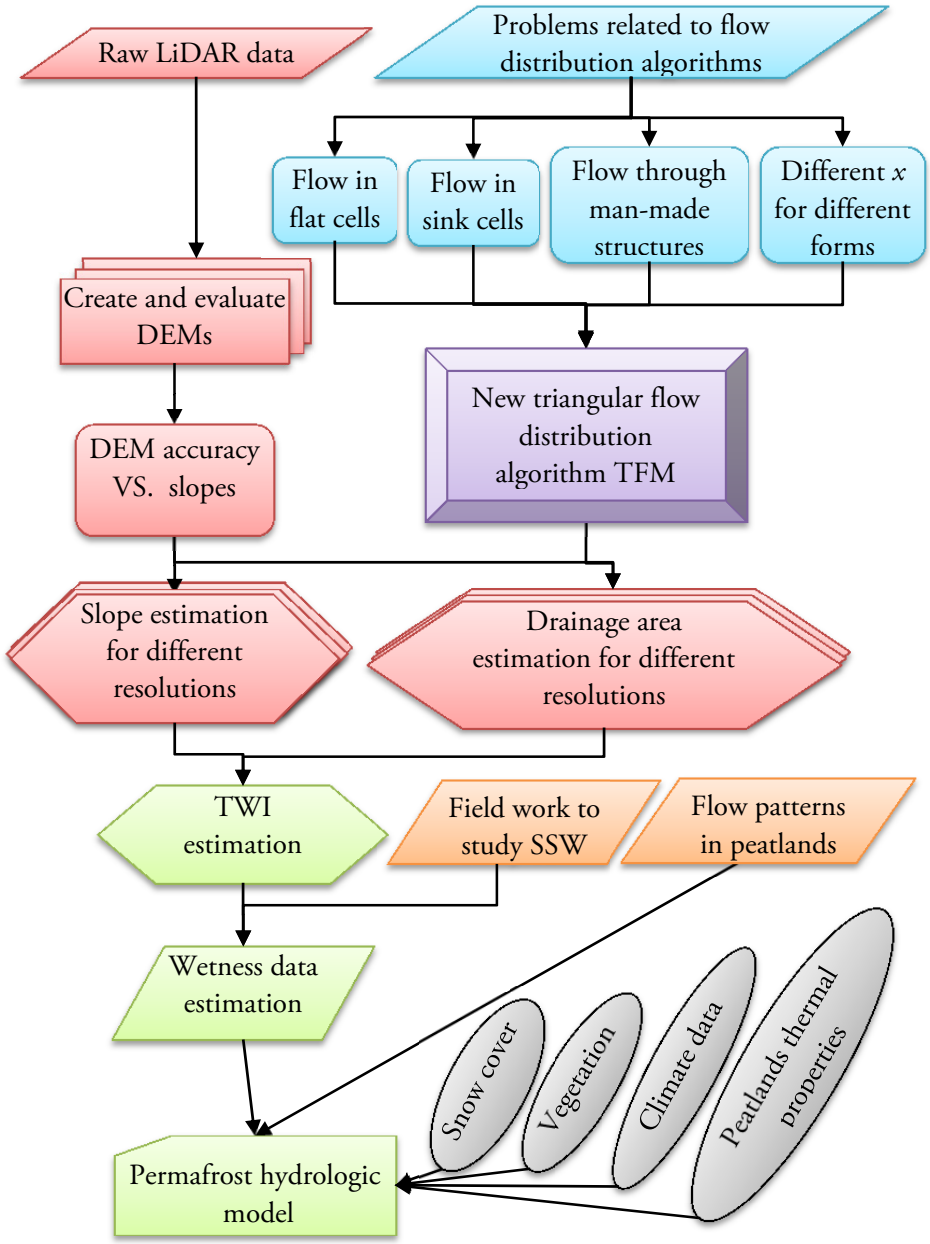

Figure 3. General study organization. The different colours demarcate the work conducted within different papers. Paper I (colour light red), paper II (colour light purple), paper III (colour light blue), paper IV (colour light orange), paper V (colour light green). Other input data layers for paper V are shaded with a light grey colour.

2.3. Digital elevation models (DEMs)

Different steps can be taken for generating DEMs. To start, we need to have measured elevation data. For the present study, DEMs were generated from LiDAR data. The evaluation data points need to be selected and excluded before generating a DEM. An interpolation algorithm is applied to estimate elevation values at each cell centre in the DEM. Finally, the DEM needs to be evaluated against ground truth evaluation data. The next five sections describe the steps we took to generate DEMs for the study area.

2.3.1. LiDAR surface elevation data

The surface elevation data used in this project are measured by an airborne LiDAR device. LiDAR is an acronym for 'Light Detection And Ranging', and is a laser-based remote sensing system used to collect various kinds of environmental data, including topographic data (Fowler, 2001). Over the area defined above the total number of the measured elevation raw data points is around 77 million. This results in a high resolution data set with an average spatial distribution of approximately 13 points/m^2. The accuracy of any LiDAR data point is related to the accuracy of the LiDAR device components (sensors). With recently developed LiDAR components, GPS and an Inertial Measurement Unit (IMU), range precision can reach 2-3 cm (Lemmens, 2007). Airborne GPS accuracy is within 5 cm horizontally and 10 cm vertically, while the accuracy of IMU is less than a couple of centimetres. For LiDAR data in general, the root mean square error (RMSE) can get 15 cm vertically and 20 cm horizontally (BC-CARMS, 2006).

The LiDAR data in the present study were retrieved with a TOPEYE S/N 425 system mounted on a Helicopter SE-HJC. The altitude when sampling was 500 m. The LiDAR data have been post-processed and adjusted against 54 known points connected to the national geodetic network. The mean vertical error after post-processing corrections is +0.4 cm, and the average magnitude of errors is 2.2 cm. The RMSE is 3.1 cm, and the standard deviation is 3.1 cm.

2.3.2. Selection of evaluation data points

Evaluation data points need to be selected before creating DEMs. The most common techniques used for the generation of evaluation points are the `leave-one-technique` within cross validation, the split-sample technique, and the independent set of sample

(Declercq 1996; Erdogan 2009; Smith et al., 2005). For our high density data we decided to use the split-sample technique. In this method, part of the raw LiDAR data is omitted before performing the interpolation.

The criterion for selecting the evaluation points was that the distance between a cell centre in the DEM that will be constructed and the selected evaluation point should be less than, or equal to, 10 mm. This enables us to validate the estimated elevations at the cell centres in the DEMs using data values that were measured at almost the same location (maximum 10 mm away from the point of interest).

The calculation of the nearest centre points, and thus the selection of evaluation data points are dependent on the resolution (cell size) of the DEM that will be created. The following six resolutions were used: 0.5, 1.0, 5.0, 10, 30, and 90 meters cell size. This implies dividing the raw data into 12 subsets, six for interpolation and six for evaluation.

2.3.3. Interpolation and DEM generation

The use of different interpolation algorithms for DEM creation has been discussed by several authors (see e.g. Anderson et al., 2005; Erdogan 2009; Lee 2003; Liu, 2008; Myers, 1994). Erdogan (2009) also investigates and reviews the role of interpolation parameters (like search radius) for the results. It is obvious that different algorithms give different results, and that some techniques are more suitable than others depending on terrain and data.

An interpolation method named the inverse distance weighted (IDW) interpolation (Shepard, 1968) is used in this study. This method is based on the assumption that an interpolated point is influenced more by nearby data points than a point further away (Burrough and McDonnell, 1998). It can be discussed if this is the most appropriate method when working in relatively flat areas, and having access to a large number of dense data points for the interpolation. Childs (2004), and Liu et al. (2007) pointed out that LiDAR data have high sampling density, and even for complex terrains the IDW approach is suitable for DEM generation, which justifies the choice. In addition, the aim of this study is not to compare different interpolation algorithms, but rather to test a commonly used one, and to look at the influence of primarily cell size on the result.

Our high density LiDAR data were used to create different resolution DEMs. Twenty-four different DEMs were created. The resolutions used were 0.5, 1, 5, 10, 30, and 90 meters. The value of the search radius when interpolating varied between four different values (1, 2, 5, and 10 meters) for each resolution (cell size). The larger

the search radius, the more data are used, and the risk of including outliers in the interpolation increases.

2.3.4. DEM evaluation

The purpose of evaluating DEMs with different resolutions is to detect possible differences, and possibly to identify the resolution that represents the evaluation data most accurately. In order to accomplish this, we calculated the deviations between the measured evaluation data points and the interpolated values for the overlapping cell centre for all combinations of resolution and search radius. Simply the differences were calculated between the predicted and measured (previously omitted) values.

The technique the most appropriate for measuring the accuracy of the DEM depends on the kind of error distribution. A normal distribution of the errors is rare in a DEM derived from data collected by LiDAR, due to e.g. filtering and interpolation errors (Höhle and Höhle, 2009). An accuracy estimation of a non-normal error distribution suggested by Höhle and Höhle (2009) was therefore used. This procedure requires the calculation of four parameters, namely the median, the normalized median absolute deviation (NMAD), and two sample quantiles.

The measurement accuracy is determined by calculating sample quantiles of the absolute differences (|Δh|), (Höhle and Höhle, 2009). Absolute errors were used because we are interested in the magnitude of the errors, and not in their signs. The sample quantiles is the order of the sample [x(1),…, x(n)], where x(1) denotes the minimum and x(n) the maximum value in the dataset. For example, the 95% sample quantile of |Δh| means that 95% of the errors have a magnitude within the interval [0; $Q_{|\Delta|}(95)$]. This means that 5% of the dataset have an error larger than the 95% quantile of |Δh|. The 50% quantile is denoted as the median. The median of the error is a robust measure, which provides or measures any systematic shift in the DEM. Moreover, the median is less sensitive to outliers in a dataset than the mean.

The NMAD is used as a measure of the standard deviation. In comparison with the standard deviation, NMAD is more resilient to outliers in the dataset (see Equation 3).

$$NMAD = 1.4826 \times median_j(\left|\Delta h_j - m_{\Delta h}\right|) \quad (3)$$

where

Δh_j denotes the individual errors j = 1,……, n and,

$m_{\Delta h}$ denotes the median of the differences in elevation.

2.3.5. Accuracy of DEM for different slope intervals

Many different authors have discussed alternative algorithms in estimation of slope from digital elevation models (see e.g. Grimaldi et al. (2007); Santini et al. (2009); Pilesjö et al. (2006); Skidmore (1989); Tang and Pilesjö (2011)). As a result, several slope calculation algorithms employed on DEMs have been used in GIS (Geography Information System) software (e.g. ARC/INFO and ERDAS IMAGINE). In this study, we have used a polynomial surface approximation. A second-order trend surface (TS), was applied on each 3 x 3 window, based on a least-square approximation. For full reference of slope estimation from a trend surface see Pilesjö et al. (1998).

In order to study the accuracy of the DEM in relation to the slope of the terrain, the evaluation points were divided into six subsets, corresponding to six slope intervals. Slopes with gradients from 0 to 50 degrees were divided into five equal intervals, while the sixth interval consisted of slopes steeper than 50 degrees. A DEM with a resolution of 0.5 m created with a search radius of 1 m was used to estimate the slope. The evaluation points were divided into six equivalent datasets, and the accuracy of the DEM was calculated for all these datasets.

2.4. Flow distribution

Each surface flow distribution and accumulation algorithm may distribute the flow using different approaches and methodologies, and may differently deal with the artefacts that normally exist in any DEM. In the following two sections a new surface flow distribution and accumulation algorithm is to be presented, and solutions for the natural and artificial artefacts (i.e. sinks, man-made structures, and flat areas), are to be demonstrated.

2.4.1. New triangular flow distribution (TFM) algorithm

The proposed triangular form-based multiple flow algorithm (TFM), presented in this study, combines the advantages of different flow distribution algorithms in a simple way. The TFM algorithm is based on multiple flow distribution allowing overland flow to all lower cells surrounding a centre cell. It is developed to be consistence for all terrain types: convex, concave, and plane terrain, as well as their combinations.

Around the midpoint (M, see Figure 4) of the cell in question (the centre cell from where the flow is estimated), eight planar triangular facets are constructed with midpoints of two adjacent cells (C1 and C2). With the aid of these eight triangular facets, our current grid cell (centre cell) is divided into eight triangular facets (Figure 4). The slope and slope direction (aspect) of each of these triangular facets can be calculated. The form of the current grid cell is represented by the combined surface of the eight triangular facets. The area of each facet is equal to 1/8 of the cell size, and represents the flow portion contributed by that facet. The overland flow of each triangular facet is to be routed out of the facet (towards other facet(s) or neighbouring cell(s)), or stays in the same triangular facet depending on slope direction.

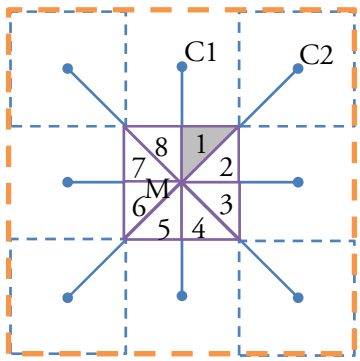

Figure 4. In a 3 by 3 cells window, the centre cell is divided into eight triangular facets (1-8). Each facet is formed from three points; one is the centre cell (M) and the two other points are two adjacent cells (e.g. C1 and C2).

We take triangular facet number one in Figure 4 as an example to explain the possible estimations of flow routing within the eight facets. The same approach will be naturally applied when estimating the flow from another of the eight facets (2-8) to its neighbouring facets.

The first step is to calculate the slope direction/aspect value for the facet intended to be analysed. Depending on the aspect value three flow routing alternatives are possible; water can be directly routed from a facet to a neighbouring cell. This alternative results in no routing to other facets and is denoted as *stay*; all water on a facet can be routed to one other neighbouring facet and is denoted as *move*; water in a facet can be routed to a neighbouring facets and a neighbouring cell, or to two neighbouring facets and is denoted as *split*. As a result of the first step, each one of the eight facets forming the cell in question will be denoted with one of the flow routing alternatives (i.e. *move, split,* or *stay*). Next we need to apply the corresponding flow-

routing alternative to the water accumulated at each facet. We start with facets denoted as *move,* and then we do facets denoted as *split*. For the facets denoted as *stay*, no action should be taken.

After doing the flow routing on each cell, consisting of eight individual facets, the routing of water to adjacent cell(s) takes place. In one or more of the eight facets water is accumulated to be routed to the neighbouring cell(s). If the centre cell represents a concave land form we can have only one facet holding all the water (directly proportional to the area, 1, of one cell), and if the cell represents a convex surface (compare a pyramid) there might be water in all eight facets.

Each facet has two neighbouring cells (see e.g. cells C1 and C2 for facet number one in Figure 4) and the next step is to distribute the flow between these cells. Two different cases can then be found:

If one neighbour cell is lower in elevation than the centre cell (where the facet is located) and the other cell is higher or equal to the centre cell, then the water accumulated in the facet will all be distributed to the lower cell.

If both neighbouring cells are lower in elevation than the centre cell, then the water accumulated in the facet will be distributed to both lower cells proportionally to slope (i.e. an x value of 1in Equation 1).

As an example to visualize the possible estimations of flow-routing within the eight facets, we use a 3 by 3 cells window (part of a saddle surface, Figure 5). The area at each facet is to be routed to other facets according to the slope direction of that facet (Figure 5B). The area accumulated in the facets is to be distributed to adjacent cells (Figure 5C).

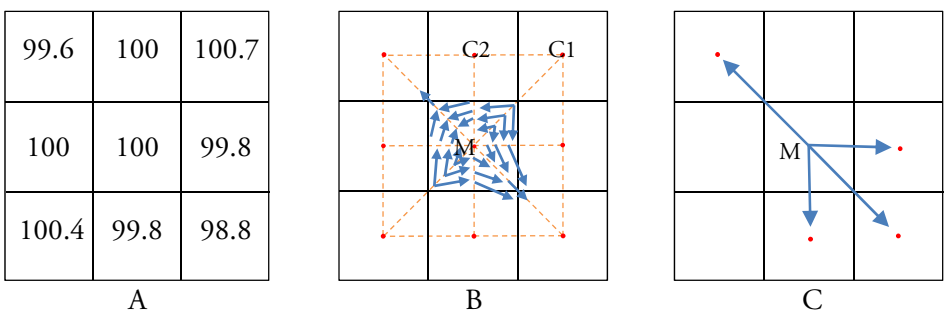

Figure 5. An illustration of a 3 by 3 cells window in a saddle surface. A) Synthetic elevation data. B) The centre cell is divided into 8 triangles. Each triangle is formed by three points: one is the centre cell (M) and the two others are any of adjacent cells like C1 and C2. C) Estimated flow directions.

The algorithm is further developed to add the possibility to deal with natural and artificial terrain artefacts, e.g. sinks, man-made structures, and flat areas. For the method as to how to deal with these artefacts, see sections 2.4.2, 2.4.3, and 2.4.4 below.

2.4.2. Filling sinks

Sinks in the DEM data might be a result of artificial artefacts, and need to be removed. In order to do this, and also include flexibility regarding area, depth and volume of the sink, a function was created in MATLAB (MathWorks, 2008). With this function, it is possible for the user to select threshold values (area, depth and volume) for sink removal through filling. The idea behind the function is rather straight forward; if we fill a sink, a flat area will be created. The number of cells in the flat area multiplied by the cell size equals the area of the sink, the maximum difference in elevation equals the depth of the sink, and the sum of all differences in elevation multiplied by the cell size equals the volume. The user is presented statistics (area, depth and volume) of the sinks, and then has the possibility to eliminate sinks of decided form and size by filling. The function also makes it possible to identify sinks which should be removed by breaching (see section 2.4.3 below).

2.4.3. Breaching break lines

Artificial artefacts in the DEM data can be man-mad structures, like roads, train lines or walls. If we know that artificial artefacts are present in the data, or we suspect their presence by visual interpretation of the DEM or by analysis of the forms and sizes of sinks (see above), there will be a need for breaching these artefacts. Thus a function to breach the cells was added, in order to enable users to deal with e.g. man-made flow barriers like roads and railway lines, or any other type of break lines. This function breaches the barrier by connecting two user-defined points/cells on the opposite sides of the obstruction. This is done in a semi-automatic way, where the user selects the approximate location of the two end points of the breach line. Then the program searches and proposes suitable points/cells (to be confirmed or changed by the user). Rules used to propose these points are that the starting point (higher elevation) should be the lowest point on the up-slope side of the barrier, and higher than the end point, being the highest point on the other side of the barrier. When the points are selected the elevation of all cells in between the points will be changed according to a linear regression line between the elevations of the starting and ending point.

2.4.4. Flat areas

Two different functions have been developed and added to the main flow distribution program in order to handle flow over flat areas.

Flat-flow-out is a function directing the flow from flat cells when a way out of the flat area can be found. Estimating the flow directions is done by routing flow over neighbouring cells to the out flow cell, and then stepwise move further and further away from the out flow cell assigning flat cells flow directions to neighbours with a defined direction (towards the outflow). Cells with the highest number of neighbours with defined flow directions are processed first, followed by cells with lower numbers of defined neighbours.

Flat-flow-in is a fuction used when there is no way out from the flat area. All cells just outside the border of the flat area have elevations higher than the flat area cells, and this result in a converging flow into the centre of the flat area. This centre cell will have no defined flow and will be treated as a sink. The flow directions of the surrounding cells will be estimated (by vector addition) starting from the flat cells that have the maximum number of known distributed flow directions cells (i.e. the border cells of the flat area).

2.5. Topographic wetness index (TWI) estimation

The estimation of TWI (Equation 2) is dependent on the estimation of drainage area and slope for each cell in the DEM, which in turn depends on the algorithms used to estimate these. The computation of the contributing drainage area A is dependent on the flow direction algorithm. Our new triangular flow direction algorithm TFM is used to calculate the upslope contributing area. The slope gradient (tan β) is estimated using trend surface method (Pilesjö et al, 1998), (see section 2.3.5).

Three different DEM resolutions were used to investigate the relationship between TWI and the DEM resolution. TWI indices (slope and drainage area) were estimated on the one hand, and the DEM resolution on the other. Resolutions of 10, 30 and 90 m were used, due to the overlapping evaluation centre cell points for these resolutions (see Figure 6 below). The slope and drainage area evaluation cells selected from the 10 and 30 m resolution DEMs are thus the ones that have the same cell centre position as the location of the 90 m resolution evaluation cells. This results in three subsets of data that have the same number of evaluation points with the same locations, but contain slope and drainage area values estimated using different DEM resolutions. The results obtained from the three subsets are then compared to identify/reveal

possible differences in the estimated slopes and drainage areas. The differences between pairs of different resolutions were calculated (i.e. 30 m -10 m, 90 m -30 m, and 90 m -10 m).

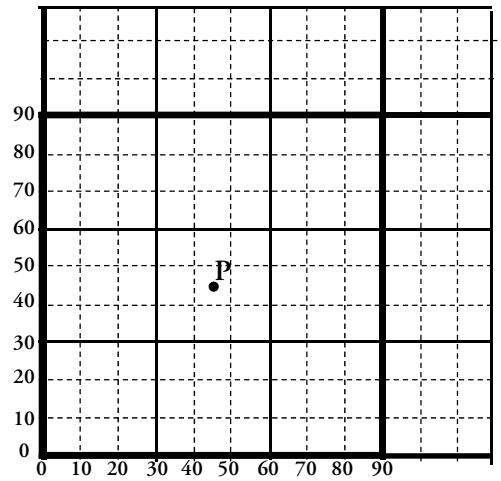

Figure 6. Point (P) is the common centre point where the 10, 30 and 90 m cell resolution cells are overlapping in a DEM.

2.6. Field work

Water level sensors were installed in the field (Stordalen mire) to conduct site specific measurements in our study area. The hydrological scheme of the field measurements consists of 30 sites where both manual measurements and continuous water level recording have been sampled in wells. The 30 sites are distributed in a way to cover most parts of the peatland mire (i.e. palsa with hollows and hummocks, internal fen and fen). Each well consists of a 2 m PVC pipe which is attached to a wooden stick, both driven as far down in the ground as possible. The pipes have got a bottom lid to prevent organic and mineral material from getting into the pipe from beneath and affect the measurements. Each pipe has 4 mm holes drilled every 10 cm, on each level four holes, for water to run freely in and out of the pipe. Since permafrost is present, the pipes were installed in late October when the active layer was as deep as possible, and they were driven down to the permafrost table.

The manual measurements were conducted biweekly after the peak of snowmelt and throughout September for the season 2010. Active layer depth was measured with a steel rod probe in the direct vicinity of the pipes. The depth to the permafrost table

inside the pipe was measured with a folding ruler that was wetted by possible water in the pipe. This gave the water table depth and the magnitude of the water above the permafrost table. Odyssey capacitive water level sensors with 1.2 m cables, and short counter weights were installed at each site to track the changes in water tables every second hour. To allow the sensors to follow the active layer as it expanded downwards over the season, the sensor's positions relative to the water table and the permafrost table were monitored weekly and adjusted by cutting the pipe to lower the sensor to the permafrost table. All cuts were logged and referenced against the wooden stick to which the pipes were attached.

2.7. **Modelling active layer thickness (ALT)**

Water content value (wetness value) is different from point to point and is highly dependent on the topography. Distributing water content accurately is important for accurate ALT estimations. In this study a permafrost hydrologic model is created to estimate the ALT for all cells in a DEM. The proposed dynamic distributed model is for modelling the effect of thawing permafrost on local topography and ALT estimation. Estimated TWI values are used to estimate how water content is distributed to all cells in the grid within the study area.

The model consists of three main parts, input datasets, main equation for the calculation of thawing depth, and the output data. Five different data inputs from different sources are required for modelling ALT. The input data in this model are: soil moisture (wetness), regional climate data, snow cover, vegetation, and the thermal properties of peat soil. The output data are estimated ALT values. Distributed wetness values were estimated from TWI values as one of the important data inputs in this model.

For the analytical representation of the ALT and the thawing of permafrost calculations, a modified Kudryavtsev's approach has been used. Kudryavtsev's approach is described thoroughly by Shiklomanov and Nelson (1999). The proposed model has a time step of one year, and can be used to simulate and predict the ALT for any number of years. The model will use the output ALT results after each time step to update the input distributed wetness.

For the running of the model, all input data were given constant values, except for the soil thermal conductivity. The thermal conductivity of the peat soil is set to be different for different cells according to its state as thawed or frozen depending on cold or warm days. Further, the thermal conductivity is different for each cell

depending on the soil water content in that cell which is estimated depending on the changes in the TWI.

3. Results and discussion

3.1. Digital elevation models (DEMs)

The generation and evaluation of different resolution DEMs from LiDAR data is one of the aims of this study. In sections 3.1.1 to 3.1.5 the results and discussion regarding the different steps are presented.

3.1.1. LiDAR surface elevation data

The scanning company delivered the LiDAR data for this study in ASCII file format that contains x, y, z data for each point. The x and y represent the coordinates of each data point while z represents the bare earth elevation at that point which is the last reflection of the scanning laser beam. Due to the large number of the scanned data points, the data were delivered in 52 files. The LiDAR data were processed in a developed MATLAB program. The developed MATLAB program was used to unify the multiple data files in order to create one data matrix, and to control the interpolation process, including the problem of processing such a large number of elevation data points.

3.1.2. Selection of evaluation data points

Selected points of evaluation to evaluate the DEMs with the six different resolutions were excluded from the original raw data. The resulting number of points is presented in the last row of Figure 7. Applying our selection criteria to the LiDAR data results in a relatively low number of selected data points for the 30 and 90 m resolutions (see Table 2). The maximum distances for the 30 and 90 m were increased to 30 and 50 mm, respectively, in order to increase the number of evaluation points, giving 230 and 68 points, instead of 57 points and 6 points, respectively. The minimum number of evaluation points should be set at 60, e.g. according to the American Society for Photogrammetry and Remote Sensing (ASPRS, 2005). The initial relatively low number of points is of course a weakness of the methodology. However, the results

obtained using the extended evaluation dataset show the same trend in errors as the evaluation using the limited number, confirming that the use of the modified selection criteria did not affect the results significantly. The extended selection was justified for statistical reasons. In this study the relative errors between different DEMs, and not the absolute errors, were in focus, which justifies the use of the LiDAR data points as ground truth, even if the errors in elevation can be up to 10 cm (see e.g. Lemmens (2007)).

Table 2. The number of selected points for each DEM resolution (Sample size) out of the total 77 million points and the NMAD for the DEMs with different combinations of resolution (cell size) and search radius (SR).

Cell size (m)	Sample size (n)	NMAD (mm)			
		1 m SR	2 m SR	5 m SR	10 m SR
0.5	154071	29.7	44.5	59.3	74.2
1	38736	29.6	44.4	59.3	88.6
5	1579	29.6	44.4	59.3	88.9
10	417	29.7	44.5	59.3	74.2
30	57(230)*	29.6	44.4	59.3	88.9
90	6(68)*	29.7	44.5	59.0	82.0

* The distance was increased at resolutions of 30 and 90 to obtain a minimum of 60 points.

3.1.3. Interpolation and DEM generation

The results from interpolating the high density LiDAR data with IDW interpolation method are twenty-four DEMs (six different DEMs, each with four different search radius). The resolutions used were 0.5, 1, 5, 10, 30 and 90 meter resolution (cell size), and four search radius values (1, 2, 5 and 10 meters) were applied. The number of interpolations was thus 24 (six resolutions times four search radiuses) as shown in Figure 7.

When choosing the different resolutions of the DEM, we logically assumed that a high resolution should reflect reality better than a lower resolution. However, it is still interesting to create and test DEMs with different resolutions since, in most cases, DEMs with lower resolutions are more commonly available, and thus more frequently used. Evaluation of the accuracy of different resolutions showed approximately the

same results regarding elevation. This was expected, since the same interpolation data set was used for all resolutions, and the evaluation points are all located close to, or very close to, the cell centres. The interpolation algorithm can then be expected to work equally well for all resolutions.

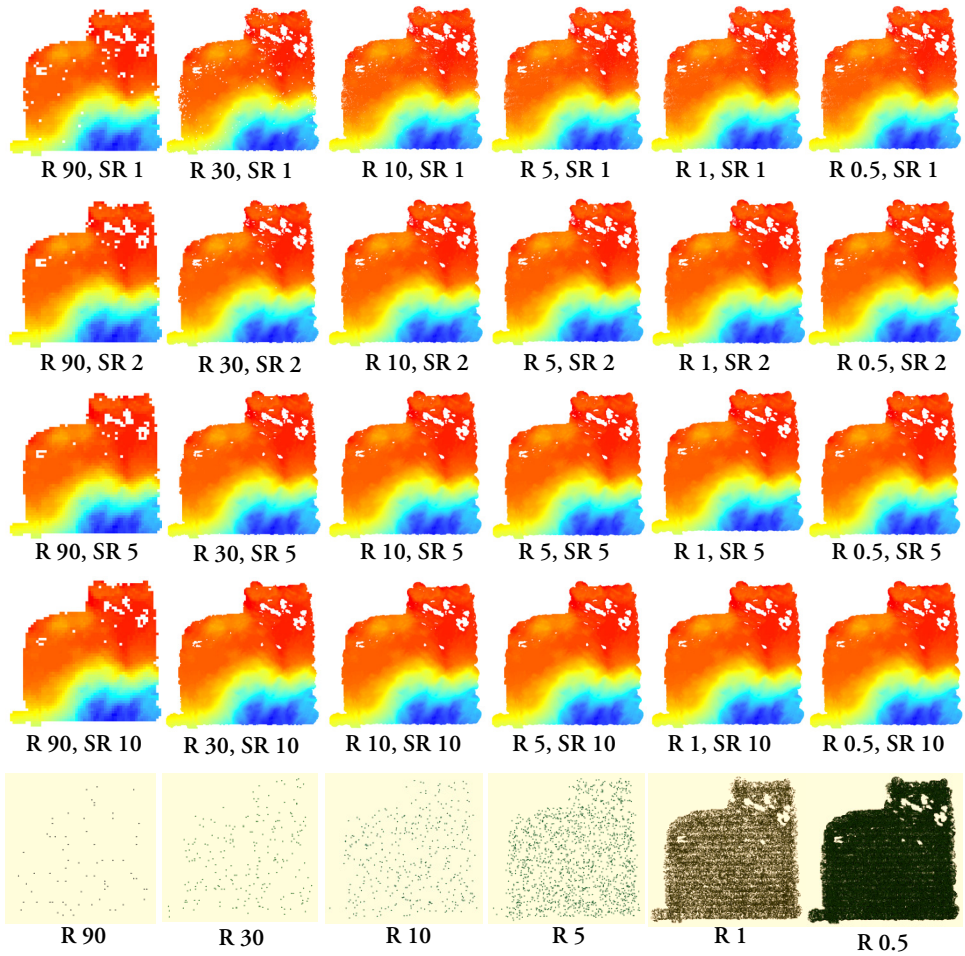

Figure 7. Digital elevation models created in six different resolutions (R) each using four different interpolation search radiuses (SR). The last row shows the evaluation data points that were excluded from the raw LiDAR data before creating the DEMs.

3.1.4. DEM evaluation

Using the robust accuracy measures appropriate for non-normal error distributions, the evaluation results of the 24 different DEMs are as follows. We calculated the median, the NMAD, and the two quantiles (68.3% and 95%) for each combination of resolution and search radius (see Table 2). The medians were all zero except for the median at 90 m resolution, which varied between -10 and -20 mm depending on the search radius. The results of the NMAD calculations indicate that the accuracy of the DEM is the same for different resolutions when using the same interpolation search radius. The accuracy is generally higher, the shorter the interpolation search radius. The results of the two quantiles confirm the NMAD results. This is an expected result, as when increasing the interpolation search radius, it can be expected to increase the errors in the created DEM. According to the measures of accuracy, the six most accurate combinations of resolution and search radius are those with the 1 m interpolation search radius. For these six cases, the maximum errors in the elevations are around 40 mm within the 68.3% quantile of the data. Moreover, the maximum errors in the DEM elevations are around 100 mm within the 95% quantile of the data.

3.1.5. Accuracy of DEM for different slope intervals

The results of evaluating the relationships between the six different slope intervals and the errors represented by the NMAD are shown in Figure 8. When visually analysing the shape of the slope error curve, it is obvious that there are larger errors in elevation when the terrain is steep than when it is flat. The first point in Figure 8A shows that for slopes between 0 and 9.99 degrees the error in elevation is around 0.03 m. Figure 8B illustrates two different quantiles of errors, also confirming that errors are larger in areas with steeper slopes.

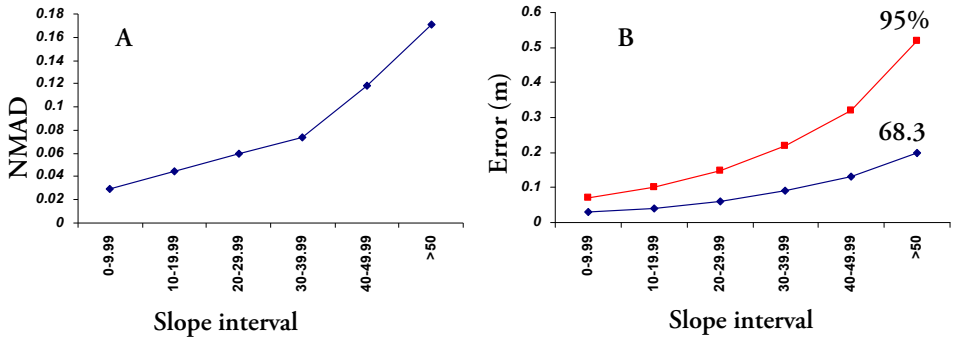

Figure 8. The relationship between the slope of the terrain and the errors in the estimated elevation. The figure A illustrates the NMAD for all data as a function of slope interval, while the figure B shows the results for the 68.3% and 95% quantiles of the errors. Both figures are based on a resolution of 0.5 m.

3.2. Flow distribution

3.2.1. New triangular flow distribution (TFM) algorithm

The flow direction of our new TFM algorithm is identical to FMFD (Freeman, 1991), and QMFD (Quinn et al., 1991), i.e. receiving cells are all lower in elevation, but the percentage of flow distributed to the cells is different. Other flow distribution algorithms are distributing the flow to one cell or more but not to all lower cells.

Figure 9 illustrates the flow distribution using different flow distribution algorithms, and also shows the percentage of flow from the centre cell to receiving cells. Following the basic rule that flow lines should always be perpendicular to contour lines (Wesseling, 1973), the flow lines on a saddle surface (Figure 9A) are drawn in Figure 9B. The results of testing our algorithm on a complex saddle surface are shown in Figure 9D, while the results from four other commonly used flow distribution algorithms are shown in Figure 9E, 9F, 9G, and 9H. From Figure 9B, one can see that 50% of the flow on this surface is supposed to be directed towards the upper left corner. The results of all flow distribution algorithms show that our new TFM algorithm (Figure 9D) is the only algorithm that gives 50% of the flow to the upper left cell. This test on a complex saddle surface demonstrates that the proposed TFM algorithm is the only algorithm that follows the logical flow direction and the percentage of distributed flow.

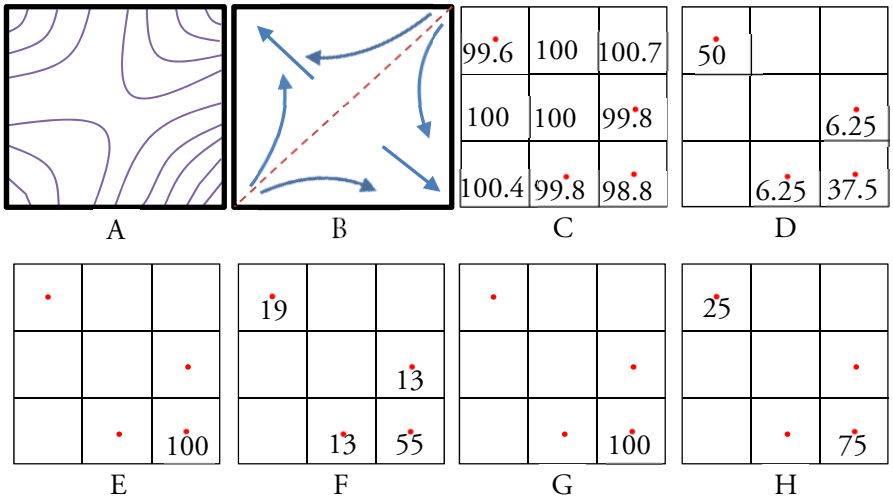

Figure 9. Distribution of flow from a centre cell to its eight neighbouring cells on a mathematical saddle surface. A) The contour lines. B) Logical flow lines. C) Synthetic elevation data. The percentage of flow distributed to neighbouring cells is as follows: D) TFM algorithm, E) D8 algorithm, F) MD8 algorithm, G) D∞ algorithm and F) MD∞ algorithm.

3.2.2. Artefacts (sinks, flat areas and break lines)

Four important functions named filling-sinks, flat-area-out, flat-area-in, and culverts were created to deal with natural and artificial artefacts (i.e. sinks, flat areas, and break lines). With the use of those four functions, it becomes possible to interactively deal with frequently existing natural and man-made (artificial) artefacts.

An interactive function for filling sinks is important when removing sinks in peatland catchment areas underlined by patchy permafrost. Sinks should not be filled automatically in order to take all the water out to the outlet, as we normally do when estimating flow routing in other flow systems without permafrost. The reason for this is that some sinks, as the one shown in Figure 13 is a natural sink, where the water is not delivered but will be evaporated or stay in small ponds until frozen layer depth is changed, which may lead to changing the topography and finding way out of this sink. With the filling-sink function, the sink can be filled according to user threshold (i.e. area, depth and volume), or the sink can be breached with culverts function if it is judged to be a sink formed by a break line. Additionally, it should be noted that with our new flat area functions, a multiple flow distribution will be estimated on flat areas. This will lead to better and more natural flow estimation.

3.3. Topographic wetness index (TWI) estimation

The results of TWI estimation are to be explained by the results of estimating the upslope contributing area (A), and the results of estimating the slope gradient (tan β) using different resolution DEMs.

3.3.1. Slope estimation using different DEM resolutions

The results of estimating slope using different DEM resolutions are obtained for the three overlapping DEMs with resolutions 90, 30 and 10 metres. Estimating slopes using different resolutions DEM shows that the medians of the differences between pairs of different resolutions (i.e. 30 m -10 m, 90 m -30 m, and 90 m -10 m) have negative signs, i.e. lower resolution (larger cell size) generates lower values of slope (Table 3). The slopes in high resolution DEMs seem to be overestimated compared to low resolution DEMs. This is logical, since smaller terrain forms, yielding larger slope estimations, will be filtered when a lower resolution is used. The NMAD and the quantile results also confirm the relationship between the slope values and the resolution. Lower resolution yields lower (less steep) slope estimations.

3.3.2. Drainage area estimation using different DEM resolutions

The results of the effect of estimating drainage area using different DEM resolutions are obtained for the three overlapping DEMs with resolutions of 90, 30 and 10 m. The medians of the differences between pairs of different resolutions (i.e. 30 m -10 m, 90 m -30 m, and 90 m -10 m) give positive signs, i.e. the lower the resolution (the larger the cell size), the higher the values of the drainage area (Table 3). This is logical, since water divides, yielding smaller drainage area estimations, will be filtered when a lower resolution is used. The NMAD and the quantile results also confirm the relationship between the values of the drainage areas and resolution. Lower resolution yields larger values in estimated drainage area.

Table 3. Measures of accuracy showing that lower slope values are obtained with lower resolution of the DEM, and higher drainage area values are obtained with lower resolution of the DEM, Sample size is equal to 2310 points.

Type of measure	30 m – 10 m	90 m – 30 m	90 m – 10 m
Difference in the median of slope (degrees)	-0.372	-0.613	-0.879
Relative slope differences	7.0%	9.0%	16%
Difference in median of drainage area (m^2)	3133	21480	29205
Relative drainage area differences	81%	83%	97%

These effects on estimated drainage area and slope, related to resolution, will be even more pronounced when calculating wetness indices, as these are normally based on the ratio between the slope and drainage area (see e.g. Sorensen et al. (2006). Thus, higher wetness indices will be predicted when you use low resolution DEMs, and relatively low values will be estimated when you use high resolution DEMs. In the present study, when changing the resolution from e.g. 10 to 30 metres, we have many examples of an increase in estimated drainage area of 50%, and a decrease of the estimated slope of 50%, resulting in a change in the estimated wetness (drainage area divided by slope) of a factor three.

Based on the results, presented above we conclude that the median of the differences in drainage area is positive, while the median of the differences in slope is negative. This indicates that high resolution DEMs will yield lower estimated values of drainage area, and higher estimated values of slope, than low resolution DEMs. Our findings of the relation between slope estimation and DEM resolution are supported by Chang and Tsai (1991), who have reported similar results for low resolution data. Zhang and Montgomery (1994) tested the grid size impact on TWI calculations, and found that a higher resolution yields better results.

TWI values were estimated using our proposed new TFN algorithm for four different resolutions (90 m, 30 m, 10, and 1m). A small part of the study area (area = 360 x 360 m) was selected to visualize the differences of the estimated TWI values between the different resolutions (Figure 10). A visual interpretation of the estimated TWI values resulted in the wetness pattern shown in Figure 10, the deeper the blue colour, the wetter the conditions.

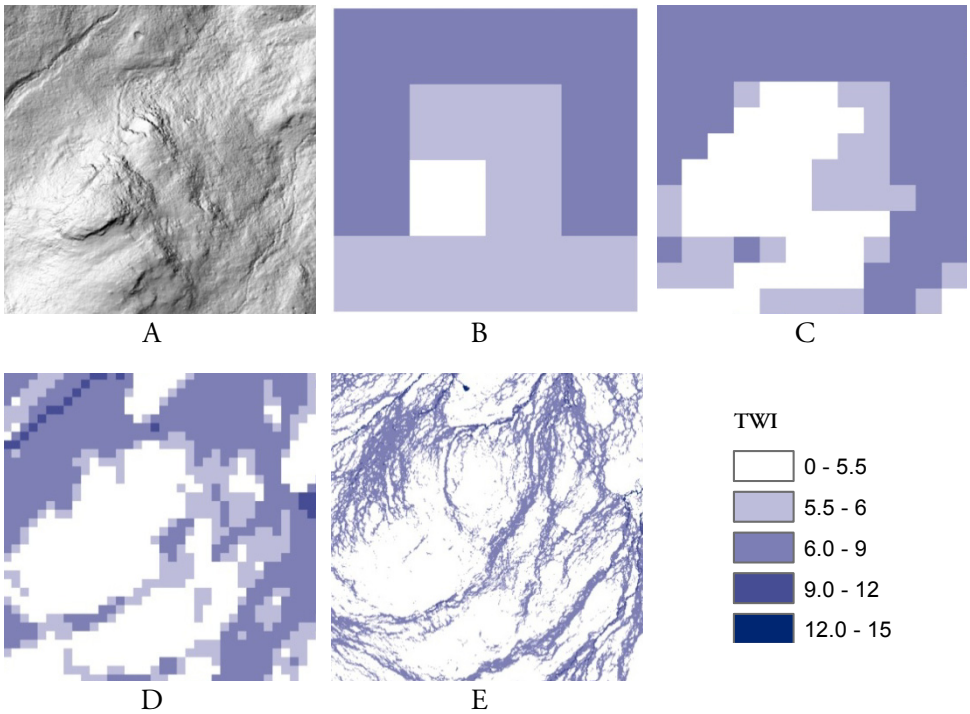

Figure 10. Topographical wetness index (TWI) estimated for different resolution DEMs. A) Hillshade of the DEM (area = 360 x 360 m). TWI estimated for the following resolutions: B) 90 m, C) 30 m, D) 10 m, E) 1 m.

The calculated mean of the estimated TWI for the same area (Figure 11) shows a decreasing trend with increasing DEM resolution, while the calculation of the standard deviation of the estimated TWI shows an increasing trend with increasing DEM resolution. The results of the calculated mean and standard deviation for the estimated TWI confirm our finding on TWI estimation for different resolution (i.e. TWI is overestimated for lower DEM resolution).

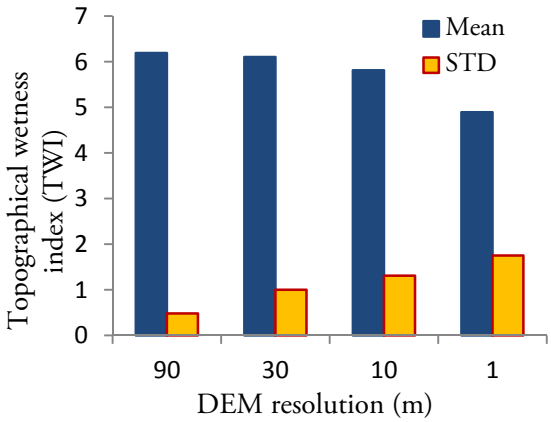

Figure 11. Calculated mean and standard deviations (STD) for TWI values estimated using different resolution DEMs.

3.4. Field work

The results of the fieldwork were divided into two parts; results from manual measurements, and the results from the water level sensors. The manual measurement results of active layer depth and water table depth were registered for two seasons. Season 1 started on the 5th of June and continued to the 26th of September 2010. For the second season, the measurements started on the 12th of June and continued to the 27th of October 2011.

The manual measurement results of active layer depth show that it is increasing for the internal fen over the whole season, and reaches a maximum of 0.5 m in the dry sites and more than 1.5 m in the wet sites. For the palsa bog area the active layer thickness and the water table depth follow each other over the season. The active layer thickness reaches a maximum of 0.5 m in this part of the peatland, while the water table depth is approximately 0.1 m measured from the bottom of the active layer throughout the season.

A plot of the manual measurements of the mean water table depths for 2010 versus an estimated (modelled) TWI is presented in Figure 12. It is shown that the estimated TWI values are higher for the fen (wet part) where the water table is near the ground surface, and lower for the plasa (dry part) where the water table is relatively deep. A visual interpretation of the TWI for the different parts of the wetland is difficult. The heterogeneity is great with similar characteristics; therefore statistical tests are

conducted for the estimated TWI, applying both the ANOVA and the t-test. The results of the plot in Figure 12 and the statistical tests confirm that estimated TWI can be used to separate (distinguish) the different types of peatland (i.e. palsa, fen, and internal fen).

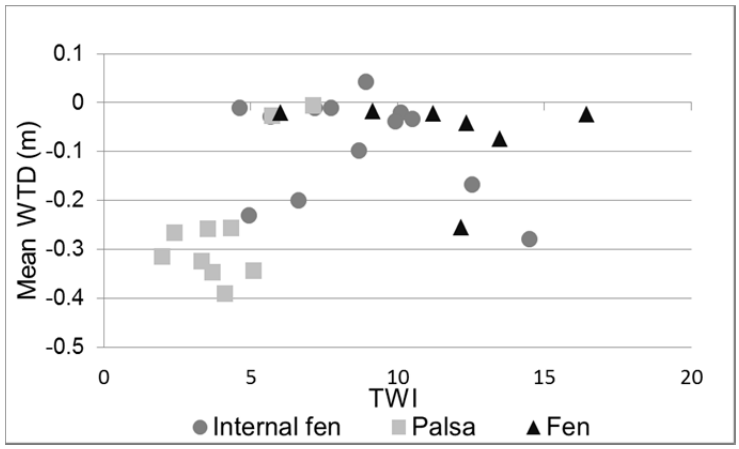

Figure. 12. Plot of the modelled TWI against the manually measured water table depth (WTD) for 2010.

From the field measurement of the study (i.e. manual and water level sensors), the flow regime above seasonally frozen layer or above permafrost has become clearer. A conceptual illustration of the flow in peatland is presented in Figure 13, showing that flow regime above seasonally frozen layer or above permafrost depends on the micro topography of a peatland.

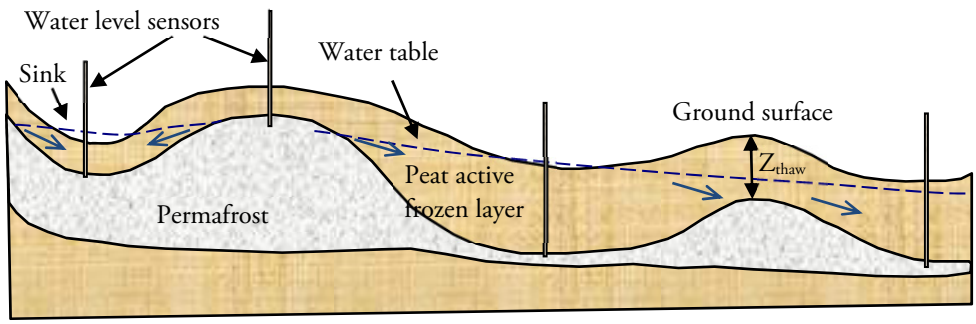

Figure 13. Conceptual illustration of flow within active layer above permafrost. The flow depends on micro topography and the active layer depth of a peatland (results from field observations and measurements).

3.5. Modelling active layer thickness

The results from running our permafrost model to estimate active layer thickness may be divided into two steps; ALT simulation and the ALT future prediction.

3.5.1. Active layer thickness (ALT) simulation

The current state of the ALT was simulated by running the permafrost model using the current mean annual air temperature at our study area equal to 0 ºC. All input data of wetness, temperature, vegetation, snow cover, and thermal characteristics were distributed to all DEM cells in our study area. The model estimates the ALT at each grid cell using the distributed input data. The estimated ALT in this model represents the maximum thawing depth in one year. The model was calibrated using our ALT field measurements.

3.5.2. Active layer thickness prediction

Following the future expectation that temperature will increase at least one degree in 100 years; the permafrost model calculation was repeated after changing the air temperature from 0 ºC to 1 ºC. The estimation of new ALT values after changing the mean annual air temperature is to demonstrate the ability of our permafrost model to predict the future ALT distribution. The predicted ALT using +1 ºC mean annual air temperature showed that changing temperature +1 ºC may increase ALT by +0.46 m.

The intention was not to use our permafrost model to estimate the exact values of ALT in each cell as real values, but to show the possibility of using an analytically based approach with semi empirical equations to estimate the maximum thawing depth of permafrost. Our study also indicates that the topographical wetness index TWI can be used to redistribute the soil water/ice content to all cells in a grid using minimum field measurements. This approach may enable us to use different input values for different cells depending on the changes in topography, which will lead to a more reliable simulation.

4.Conclusions

In accordance with the objectives, the main conclusions of this study are presented below.

Regarding the relation between DEMs generated from high resolution LiDAR data and topographical derivatives (e.g., drainage area, slope, and wetness) we can conclude that:

1. The estimates of the slope and drainage area, and thus also the topographic wetness index, differ significantly with the resolution of the digital elevation model. Slope values become lower and drainage areas values become higher when the resolution decreases (i.e. cell size is increasing).

2. The search radius, but not cell size, significantly influences the accuracy of a DEM, and that the accuracy is generally higher the shorter the interpolation search radius.

3. The accuracy of the DEM differs significantly with the slope of the terrain, and that the errors in elevation are larger when the terrain is steep compared to when it is flat.

Regarding flow distribution algorithms we can conclude that our newly created flow distribution algorithm supported by artefact removal functions works well to estimate flow over both mathematical and natural surfaces, compared to other tested algorithms.

The field work water level measurements led to better understanding of flow regime in peatlands, especially when they are underlain by a seasonally frozen layer or permafrost. The field work also helped to confirm that estimated wetness using the proposed flow routing algorithm on digital elevation model can be used to distribute wetness to all cells in a DEM.

Additionally, the study has shown the possibility of using an analytically based approach together with semi-empirical equations to estimate the maximum thawing depth (active layer thickness) above permafrost.

5.References

ACIA (2005) Arctic Climate Impact Assessment Cambridge University press, New York, USA.

Akerman H J and Johansson M (2008) Thawing permafrost and thicker active layers in sub-arctic Sweden. Permafrost and Periglacial Processes, 19, 279-292.

Anderson ES, Thompson JA, Austin RE (2005) LIDAR density and linear interpolator effects on elevation estimates. Int J Remote Sens 26: 3889-3900 DOI 10.1080/01431160500181671

Andersson NÅ, Callaghan TV, Karlsson PS (1996) The Abisko Scientific Research Station. Ecological Bulletins: 11-14, 15

ASPRS (2005) ASPRS Guidelines, Vertical Accuracy Reporting for Lidar Data In: Sensing ASfPaR (ed) Geospatial Solutions, pp. 56-56.

Baird AJ, Belyea LR, Morris PJ (2009) Upscaling of Peatland-Atmosphere Fluxes of Methane: Small-Scale Heterogeneity in Process Rates and the Pitfalls of "Bucket-and-Slab" Models Carbon Cycling in Northern Peatlands, 184 edn, Geophysical Monograph Series:37-53.

Barling RD, Moore ID, Grayson RB (1994) A quasi-dynamic wetness index for characterizing the spatial distribution of zones of surface saturation and soil water content. Water Resources Research 30: 1029-1044

BC-CARMS (2006) LiDAR – overview of technology, applications, market features and industry. Victoria, BC: Centre for Applied Remote Sensing, Modelling and Simulation, University of Victoria

Beven KJ, Jakeman AJ (1988) Complexity and uncertainty in predictive models. In: G. DD (ed) Intl Symposium on Water Quality Modeling of Agricultural Non-Point Sources, pp. 555-576.

Beven KJ, Kirkby MJ (1979) A physically based, variable contributing area model of basin hydrology. Hydrological Sciences Journal 24: 43-69

Bosiö J, Johansson M, Callaghan T, Johansen B and Christensen T (2012) Future vegetation changes in thawing subarctic mires and implications for greenhouse gas exchange—a regional assessment. Climatic Change, Acceped(http://dx.doi.org/10.1007/s10584-012-0445-1): 1-20.

Burrough P, A., McDonnell R, A. (1998) Principles of Geographical Information Systems Oxford University Press, Oxford

Chang KT, Tsai BW (1991) The effect of DEM resolution on slope and aspect mapping. Cartography and Geographic Information Systems 18: 69-77 DOI 10.1559/152304091783805626

Childs C (2004) Interpolation surfaces in ArcGIS spatial analyst. ArcUser July–September

Christensen TR, Johansson T, Akerman HJ, Mastepanov M, Malmer N, Friborg T, Crill P, Svensson BH (2004) Thawing sub-arctic permafrost; effects on vegetation and methane emissions. Geophysical Research Letters 31

Costa-Cabral MC, Burges SJ (1994) Digital elevation model networks (DEMON): A model of flow over hillslopes for computation of contributing and dispersal areas. Water Resources Research 30: 1681-1692

Curmi P, Durand P, Gascuel Odoux C, Merot P, Walter C, Taha A (1998) Hydromorphic soils, hydrology and water quality: spatial distribution and functional modelling at different scales. Nutrient Cycling in Agroecosystems 50: 127-142

Declercq FAN (1996) Interpolation Methods for Scattered Sample Data: Accuracy, Spatial Patterns, Processing Time. Cartography and Geographic Information Science 23: 128-144 DOI 10.1559/152304096782438882

Erdogan S (2009) A comparision of interpolation methods for producing digital elevation models at the field scale. Earth Surf Process Landf 34: 366-376 DOI 10.1002/esp.1731

Fairfield J, Leymarie P (1991) Drainage networks from grid digital elevation models. Water Resources Research 27: 709-717 DOI 10.1029/90wr02658

Famiglietti JS, Rudnicki JW, Rodell M (1998) Variability in surface moisture content along a hillslope transect: Rattlesnake Hill, Texas. Journal of Hydrology 210: 259-281 DOI 10.1016/s0022-1694(98)00187-5

Famiglietti JS, Wood EF (1991) Evapotranspiration and runoff from large land areas - land surface hydrology for atmospheric general-circulation models. Surveys in Geophysics 12: 179-204 DOI 10.1007/bf01903418

Fowler R (2001) Topographic Lidar In: Maune D (ed) Digital Elevation Model Technologies And Applications:p. 207-236.

Freeman TG (1991) Calculating catchment area with divergent flow based on a regular grid. Computers and Geosciences 17: 413-422

Frolking S, Roulet NT (2007) Holocene radiative forcing impact of northern peatland carbon accumulation and methane emissions. Global Change Biology 13: 1079-1088

Gedney N, Cox PM (2003) The sensitivity of global climate model simulations to the representation of soil moisture heterogeneity. Journal of Hydrometeorology 4: 1265-1275

Grimaldi S, Nardi F, Di Benedetto F, Istanbulluoglu E, Bras RL (2007) A physically-based method for removing pits in digital elevation models. Adv Water Resour 30: 2151-2158 DOI 10.1016/j.advwatres.2006.11.016

Guntner A, Seibert J, Uhlenbrook S (2004) Modeling spatial patterns of saturated areas: An evaluation of different terrain indices. Water Resources Research 40 DOI W05114 10.1029/2003wr002864

Hinzman LD, Kane DL, Woo M-k (2006) Permafrost HydrologyEncyclopedia of Hydrological Sciences.

Höhle J, Höhle M (2009) Accuracy assessment of digital elevation models by means of robust statistical methods. ISPRS Journal of Photogrammetry and Remote Sensing 64: 398-406

Holmgren P (1994) Multiple flow direction algorithms for runoff modelling in grid based elevation models: an empirical evaluation. Hydrological Processes 8: 327-334

Holmgren P (1994) Topographic and geochemical influence on the forest site quality, with respect to Pinus sylvestris and Picea abies in Sweden. Scandinavian Journal of Forest Research 9: 75-82

Johansson T, Malmer N, Crill PM, Friborg T, Akerman JH, Mastepanov M, Christensen TR (2006) Decadal vegetation changes in a northern peatland, greenhouse gas fluxes and net radiative forcing. Global Change Biology 12: 2352-2369

Kirkby MJ, Kneale PE, Lewis SL, Smith RT (1995) Modelling the form and distribution of peat mires. In: Hughes JMR, Heathwaite AL (eds) Hydrology and Hydrochemistry of British Wetlands:83-93.

Lee HS (2003) A hybrid model for DTM generation from LiDAR signatures. PhD thesis, Mississippi State University

Lemmens M (2007) Airborne LiDAR sensors. GIM International 21(2): 24–27

Liu XY (2008) Airborne LiDAR for DEM generation: some critical issues. Prog Phys Geogr 32: 31-49 DOI 10.1177/0309133308089496

Liu XY, Zhang ZY, Peterson J, Chandra S (2007) LiDAR-derived high quality ground control information and DEM for image orthorectification. Geoinformatica 11: 37-53 DOI 10.1007/s10707-006-0005-9

MathWorks (2008) MATLAB, R2008B edn MathWorks, Natick, Massachusetts.

Moore ID, Norton TW, Williams JE (1993) Modeling environmental heterogeneity in forested landscapes. Journal of Hydrology 150: 717-747 DOI 10.1016/0022-1694(93)90133-t

Myers DE (1994) Spatial interpolation - an overview. Geoderma 62: 17-28 DOI 10.1016/0016-7061(94)90025-6

O'Callaghan JF, Mark DM (1984) The extraction of drainage networks from digital elevation data. Computer Vision, Graphics, and Image Processing 28: 323-344

O'Loughlin EM (1986) Prediction of surface saturation zones in natural catchments by topographic analysis. Water Resources Research 22: 794-804

Olefeldt D, Roulet NT (2012) Effects of permafrost and hydrology on the composition and transport of dissolved organic carbon in a subarctic peatland complex. J Geophys Res 117: G01005 DOI 10.1029/2011jg001819

Orlandini S, Moretti G, Franchini M, Aldighieri B, Testa B (2003) Path-based methods for the determination of nondispersive drainage directions in grid-based digital elevation models. Water Resour Res 39: 1144 DOI 10.1029/2002wr001639

Parsons AJ, Abrahams AD (1992) Overland Flow: Hydraulics And Erosion Mechanics UCL Press

Pilesjö P, Persson A, Harrie L (2006) Digital elevation data for estimation of potential wetness in ridged fields-Comparison of two different methods. Agricultural Water Management 79: 225-247

Pilesjö P, Zhou Q, Harrie L (1998) Estimating flow distribution over digital elevation models using a form-based algorithm. Geographic Information Sciences 4: 44-51

Quinn P, Beven K, Chevallier P, Planchon O (1991) The prediction of hillslope flow paths for distributed hydrological modelling using digital terrain models. Hydrological Processes 5: 59-79

Robson A, Beven K, Neal C (1992) Towards identifying sources of subsurface flow - a comparison of components identified by a physically based runoff model and those determined by chemical mixing techniques. Hydrological Processes 6: 199-214 DOI 10.1002/hyp.3360060208

Rodhe A, Seibert J (1999) Wetland occurrence in relation to topography: A test of topographic indices as moisture indicators. Agricultural and Forest Meteorology 31: 98-99

Rydén BE, Fors L, Kostov L (1980) Physical properties of the tundra soil-water system at Stordalen, Abisko. In: Sonesson M (ed) Ecology of a Subarctic Mire, Ecological Bulletins 30.

Santini M, Grimaldi S, Nardi F, Petroselli A, Rulli MC (2009) Pre-processing algorithms and landslide modelling on remotely sensed DEMs. Geomorphology 113: 110-125 DOI 10.1016/j.geomorph.2009.03.023

Schmidt F, Persson A (2003) Comparison of DEM Data Capture and Topographic Wetness Indices. Precision Agriculture 4: 179-192

Seibert J, McGlynn BL (2007) A new triangular multiple flow direction algorithm for computing upslope areas from gridded digital elevation models. Water Resour Res 43: W04501 DOI 10.1029/2006wr005128

Shepard D (1968) A two-dimensional interpolation function for irregularly-spaced data. Paper presented at the The 1968 23rd ACM national conference1968

Shiklomanov NI, Nelson FE (1999) Analytic representation of the active layer thickness field, Kuparuk River Basin, Alaska. Ecological Modelling 123: 105-125 DOI 10.1016/s0304-3800(99)00127-1

Sivapalan M, Wood EF (1987) A multidimensional model of nonstationary space-time rainfall at the catchment scale. Water Resources Research 23: 1289-1299 DOI 10.1029/WR023i007p01289

Skidmore AK (1989) A comparison of techniques for calculating gradient and aspect from a gridded digital elevation model. International Journal of Geographical Information Systems 3: 323-334

Smith SL, Holland DA, Longley PA (2005) Quantifying interpolation errors in urban airborne laser scanning models. Geogr Anal 37: 200-224 DOI 10.1111/j.1538-4632.2005.00636.x

Sonesson M, Jonsson S, Rosswall T, Rydén BE (1980) The Swedish IBP/PT Tundra Biome Project Objectives-Planning-Site. Ecological Bulletins: 7-25

Sorensen R, Zinko U, Seibert J (2006) On the calculation of the topographic wetness index: evaluation of different methods based on field observations. Hydrology and Earth System Sciences 10: 101-112

Tang J, Pilesjö P (2011) Estimating slope from raster data: a test of eight different algorithms in flat, undulating and steep terrain. In: BREBBIA CA (ed) River Basin Management VI Wessex Institute of Technology, UK, Riverside, California, USA, pp. 143-154.

Wania R, Ross I, Prentice IC (2010) Implementation and evaluation of a new methane model within a dynamic global vegetation model: LPJ-WHyMe v1.3.1. Geoscientific Model Development 3: 565-584 DOI 10.5194/gmd-3-565-2010

Wesseling J (1973) Drainage principles and application. Vol. II. Theories of field drainage and watershed runoff. 13. Seepage. Publication, International Institute for Land Reclamation and Improvement: 189-222

Wolock DM, McCabe GJ (1995) Comparison of single and multiple flow direction algorithms for computing topographic parameters in TOPMODEL. Water Resources Research 31: 1315-1324

Woo MK (2012) Permafrost Hydrology. Springer

Zhang T, Barry RG, Knowles K, Ling F, Armstrong RL (2003) Distribution of seasonally and perennially frozen ground in the Northern Hemisphere

Zhang WH, Montgomery DR (1994) Digital elevation model grid size, landscape representation, and hydrologic simulations. Water Resour Res 30: 1019-1028 DOI 10.1029/93wr03553

Zhou Q, Lees B, Tang GA (2008) Advances in Digital Terrain Analysis. Springer

Zhou Q, Liu X (2002) Error assessment of grid-based flow routing algorithms used in hydrological models. Int J Geogr Inf Sci 16: 819-842

Zhou Q, Pilesjö P, Chen Y (2011) Estimating surface flow paths on a digital elevation model using a triangular facet network. Water Resour Res 47: W07522 DOI 10.1029/2010wr009961